Direct Relationship between Protein Expression and Progeny Yield of Herpes Simplex Virus 1 Unveils a Rate-limiting Step for Virus Production

Moeka Nobe[1,7], Yuhei Maruzuru[1,2,3,7], Kosuke Takeshima[1,2,3], Fumio Maeda[4], Hideo Kusano[4], Raiki Yoshimura[5], Takara Nishiyama[5], Hyeongki Park[5], Yoshitaka Kozaki[5], Shingo Iwami[5], Naoto Koyanagi[1,2,3], Akihisa Kato[1,2,3], Tohru Natsume[4], Shungo Adachi[4], and Yasushi Kawaguchi[1,2,3,6]

[1]Division of Molecular Virology, Department of Microbiology and Immunology, The Institute of Medical Science, The University of Tokyo, Tokyo, Japan

[2]Department of Infectious Disease Control, International Research Center for Infectious Diseases, The Institute of Medical Science, The University of Tokyo, Minato-ku, Tokyo 108-8639, Japan

[3]Research Center for Asian Infectious Diseases, The Institute of Medical Science, The University of Tokyo, Tokyo, Japan

[4]Molecular Profiling Research Center for Drug Discovery (molprof), National Institute of Advanced Industrial Science and Technology (AIST), Tokyo, 135-0064, Japan.

[5]Interdisciplinary Biology Laboratory (iBLab), Division of Biological Science, Graduate School of Science, Nagoya University, Nagoya 464-8602, Japan

[6]The University of Tokyo, Pandemic Preparedness, Infection and Advanced Research Center, Tokyo, Japan

*Address correspondence to:
Dr. Yasushi Kawaguchi
Division of Molecular Virology
Department of Microbiology and Immunology
The Institute of Medical Science
The University of Tokyo
4-6-1 Shirokanedai, Minato-ku, Tokyo 108-8639, Japan

Phone: 81-3-6409-2070
Fax: 81-3-6409-2072
E-mail: ykawagu@ims.u-tokyo.ac.jp

[7]These authors contributed equally to this work.

ABSTRACT

Although viral protein expression and progeny virus production were independently shown to be highly heterogenous in individual cells, their direct relationship, analyzed by considering their heterogeneities, has not been investigated to date. This study established a system to fractionate cells infected with a herpesvirus based on the levels of the global expression of viral late proteins, which are largely virion structural proteins, and to titrate virus yields in these fractions. This system demonstrated a direct relationship and indicated there was a threshold for the levels of viral late protein expression for progeny virus production and that viral DNA cleavage/packaging was a rate-limiting step for progeny virus production. These findings, which were masked in previous studies performed at the entire population level, have uncovered a sophisticated viral strategy for efficient progeny virus production and shed new light on an effective target for the development of anti-viral drugs.

INTRODUCTION

The state of viral gene expression has long been thought to be one of the critical determinants for virus progeny production [1]. Viral infection is usually studied at the entire population level by averaging the outcomes of infection from each of large numbers of individual cells. In these previous studies, a relationship between viral gene expression and virus progeny production has necessarily been investigated based on classical time course experiments in which levels of viral gene expression and progeny virus titers were compared at various times after infection. Such studies demonstrated that the levels of viral gene expression, including the expressions of viral mRNA and protein, correlated well with progeny virus yields [2-6]. However, accumulating evidence has indicated that viral infection at the single-cell or subpopulation level is highly heterogeneous, which has been masked in studies performed at the entire population level. Thus, it was reported that the progeny virus yield from individual cells spanned several orders of magnitude [7-14]. Classical fluorescence microscopy and recent advances in single-cell RNA-sequencing have enabled the investigation of the state of viral gene expression at the single-cell level, revealing high heterogeneity in individual cells and identifying new subpopulations of infected cells with similar viral gene expression profiles [15-17]. However, the use of single-cell analyses to investigate both viral gene expression and progeny virus production is

69 limited. Thus, single-cell analyses for both viral RNA synthesis and progeny virus
70 production have been reported for some RNA viruses [10, 12, 14]; a recent study reported that
71 influenza virus transcription and progeny virus production were poorly correlated at the
72 single cell level [14], and other studies did not focus on the relationship between viral
73 transcription and virus progeny production at the single cell level [10, 12]. Furthermore, there
74 is a lack of information on viral protein expression and virus progeny production in the
75 same individual cell or subpopulation. Therefore, the direct relationship between viral
76 protein expression and progeny virus production, analyzed by considering their
77 heterogeneities at single cell or subpopulation levels, remains to be elucidated. These
78 observations raised a fundamental question as to whether the well-established correlation
79 between viral protein expression and progeny virus production detected at the entire
80 population level by classical time-course experiments [4, 6] does reflect a direct relationship
81 between them.

82 Herpes simplex virus 1 (HSV-1), an extensively studied DNA virus, is a
83 ubiquitous human pathogen, causing a variety of diseases including encephalitis, keratitis,
84 and mucocutaneous and skin diseases including herpes labialis, genital herpes and
85 herpetic whitlow [18]. HSV-1 encodes more than 100 different proteins [19-21] and HSV-1
86 genes fall into three major classes: immediate-early (IE), early (E) and late (L), whose

expressions are coordinately regulated and sequentially ordered in a cascade during lytic infection [19]. Although there are some exceptions, virion structural proteins are largely encoded by L genes [19]. Replication of the HSV-1 genome and packaging of the replicated viral genomes into nascent capsids occurs in the nucleus [19]. Nascent nucleocapsids are exported to the cytoplasm through the perinuclear space between the inner nuclear membrane and outer nuclear membrane by a nuclear pore-independent and sequential envelopment/de-envelopment process [19]. In the cytoplasm, capsids acquire a final envelope by budding into cytoplasmic vesicles and become infectious [19].

In this study, we constructed a reporter HSV-1 to monitor the global expression of viral L proteins by analyzing direct and quantitative relationship between L protein expression levels and virus progeny yields by sorting infected cells into subpopulations based on reporter gene expression levels and by determining virus titers in the subpopulations. The clarified relationship indicated a threshold in the levels of HSV-1 L protein expression for progeny virus production, demonstrating viral DNA cleavage/packaging is a rate-limiting step for progeny virus production.

RESULTS

Construction and characterization of a reporter HSV-1 to analyze viral L protein expression and virus progeny yields at the subpopulation level. We constructed a recombinant virus rICP47/vUs11 expressing IE protein ICP47 and L protein Us11 fused to monomeric fluorescent proteins, TagRFP and VenusA206K (TagRFP-ICP47 and Venus-Us11), respectively (Fig. 1A and B). The growth of rICP47/vUs11 was similar to wild-type HSV-1(F) in HeLa cells at a multiplicity of infection (MOI) of 5 and reached a plateau 24 h after infection (Fig. 1C). Flow cytometric analyses showed 92% of HeLa cells inoculated with rICP47/vUs11 at an MOI of 5 were TagRFP positive 24 h after inoculation, indicating that in these experimental settings, most HeLa cells were infected with rICP47/vUs11 and HSV-1 gene expression was initiated in these infected cells (Fig. 1D and E). Frequencies of cells positive for Venus and TagRFP, or those positive for TagRFP and negative for Venus, were 67% and 25%, respectively (Fig. 1E). Cells positive for Venus and negative for TagRFP were barely detectable (Fig. 1D and E). Notably, the coefficient of variation (CV) for Venus-Us11 fluorescence intensities in each infected cell was significantly higher than for TagRFP-ICP47 fluorescence (Fig. 1F).

To examine whether levels of Venus-Us11 fluorescence in rICP47/vUs11-infected cells were related to those of the global expression of HSV-1 L proteins, HeLa

cells infected with rICP47/vUs11 at an MOI of 5 for 24 h were analyzed by flow cytometry and sorted into six subpopulations (f1 to f6) based on the levels of Venus-Us11 fluorescence intensities—Venus-Us11 fluorescence intensities increased in subpopulations from f1–f6 (S-Fig. 1A). The subpopulations were then subjected to LC-MS/MS to quantitate peptides of global HSV-1 L proteins (Fig. 2A and S-Fig. 1B). There was a strong correlation between the levels of Venus-Us11 fluorescence intensities and the relative abundance of each of 49 HSV-1 L proteins including Venus-Us11 (43 L proteins, r>0.93; 6 L proteins, r>0.85; Fig. 2B). These results suggested that Venus-Us11 fluorescence intensities reflected expression levels of global HSV-1 L proteins in rICP47/vUs11-infected cells.

Specific Venus-Us11 protein expression levels are linked to progeny virus production. To analyze a relationship between expression levels of HSV-1 L proteins and progeny virus yields directly and quantitatively, HeLa cells were infected with rICP47/vUs11 at an MOI of 5, harvested at 4, 6, 8, 10, 12, and 24 h after infection, analyzed by flow cytometry and sorted into entire population (FSC singlet) or six subpopulations (f1 to f6) according to the levels of Venus-Us11 fluorescence intensity (S-Fig. 2). Virus titers in the entire population and each of the subpopulations were determined and virus titers per 10^4 cells were estimated.

In agreement with previous reports [4, 6], the kinetics of Venus-Us11 fluorescence intensity were similar to those of progeny virus titers (Fig. 3A) and Venus-Us11 fluorescence intensities had a high correlation with progeny virus titers at the entire population level (r=0.94) (Fig. 3B). We also calculated virtual titers per 10^4 cells at each timepoint by summating virus titers in subpopulations, obtained by multiplying the estimated virus titer of each subpopulation of 10^4 cells by the ratio of number of cells in the subpopulation to that in the entire population. A viral growth curve based on the virtual titers was similar to that based on actual titers in the entire population (Fig. 3C).

At the entire population level, virus titers were decreased 6 h after infection due to an eclipse phase of infection and viral replication entered the productive phase between 6 and 8 h post-infection (Fig. 3A and C). These results indicated that infectious progeny virus production was detectable 8 h after infection in these experiments. The f4 subpopulation emerged at this timepoint (Fig. 3D and E). Although 4.1% of total cells were in the f4 subpopulation 8 h after infection (Fig. 3E), 55% of progeny infectious virus yields were produced by this subpopulation (Fig. 3F). The f5 and f6 subpopulations emerged 10 and 12 h after infection, respectively, when the growth rate had slowed (Fig. 3D and E). At 10 h after infection, 18% of total cells were in the f4 and f5 subpopulations (Fig. 3E) and these subpopulations produced 87% of progeny infectious virus yields (Fig.

3F). At 12 and 24 h post-infection, 33% and 53% of total cells were in the f4 to f6 subpopulations, respectively (Fig. 3E), and these subpopulations produced 95% of progeny infectious virus yields (Fig. 3F). Similar results in HeLa cells at an MOI of 5 at 24 h post-infection were obtained with these cells using MOIs of 1 and 2.5 at this timepoint, and with other cells (Vero and U2OS cells) (S-Fig. 3).

Next, we analyzed virion morphogenesis by quantitating the number of virus particles at different morphogenetic stages in HSV-1-infected HeLa cells at an MOI of 5 for 24 h in each subpopulation f2 to f5 by electron microscopy. All virion types were barely detectable in infected cells from subpopulation f2 (Fig. 4). In subpopulation f3, although nuclear virions were obvious, cytoplasmic virions, and especially enveloped virions in the cytoplasm that were considered infectious, were barely detectable (Fig. 4). In contrast, enveloped virions were detected in the cytoplasm of 70% and 100% of infected cells in the f4 and f5 subpopulations, respectively (Fig. 4).

These results together with the observation that Venus-Us11 fluorescence intensities reflected expression levels of global HSV-1 L proteins indicated that (i) subpopulations f4 to f6 have a predominant role in yielding progeny infectious viruses, whereas subpopulations f1 to f3 barely produced infectious virions, (ii) a threshold of progeny virus production existed between Venus-Us11 protein expression levels in

subpopulations f3 and f4, and (iii) certain levels of L protein expression were required for progeny virus production. Cells in the f1 to f3 subpopulations were likely to be aborted infected cells and their frequencies 24 h after infection were similar to those reported previously in HeLa cells [13, 22].

Notably, Venus-Us11 fluorescence intensities in subpopulations above the threshold (f4 to f6) correlated highly with progeny virus titers (r=0.93) (Fig. 3G). In contrast, a much lower correlation of coefficient (r=0.48) was observed in subpopulations below the threshold (Fig. 3G). Furthermore, virus titers in subpopulations f4 to f6 remained unchanged during HSV-1 infection (Fig. 3H) indicating virus titers in subpopulations above the threshold were determined by L protein expression levels independent of the timepoint after infection. Thus, infectious progeny virus production in the entire population depended on the proportion of these subpopulations.

Virion morphogenesis with a defect in the cleavage/packaging of HSV-1 DNA genome occurs in the subpopulation below the threshold for progeny virus production. The threshold for progeny virus production detected between Venus-Us11 protein expression levels in subpopulations f3 and f4 suggested a rate-limiting viral step for progeny virus production. Conceivably, this defect(s) might be observed in subpopulations below the threshold (f1 to f3) but not in subpopulations above the

threshold (f4 to f6). To clarify this rate-limiting viral step, we compared levels of HSV-1 DNA genome replication and global viral mRNA expression in subpopulations f1 to f6 by quantitative PCR and RNA sequencing, respectively. Amounts of HSV-1 genome DNA increased in the f1 subpopulation and almost reached a plateau between subpopulations f2 and f3 (S-Fig. 4A). Similar proliferative profiles were observed for expressions of each of the 70 HSV-1 mRNAs tested (S-Fig. 4B). Thus, we did not detect any rate-limiting effects of HSV-1 genome replication or viral mRNA expression associated with the threshold for progeny virus production.

Next, we visualized virion morphogenesis by electron microscopy focusing on the A, B and C capsids in the nucleus (Fig. 5 and S-Fig. 5). The A and B capsids are incomplete structures resulting from problems in viral DNA genome retention in the capsids and packaging into the capsids, respectively [23-25]. C capsids are mature capsids (nucleocapsids) containing viral DNA genomes reported to be selectively exported to the cytoplasm [26-29]. B capsids accumulated aberrantly in subpopulation f3 and most (90.1%) nuclear capsids in this subpopulation were B capsids (Fig. 5 and S-Fig. 5). The frequency of B capsids in subpopulation f3 was significantly higher than in subpopulations f4 and f5 (Fig. 5B). In contrast, the frequency of C capsids in subpopulation f3 was significantly lower than in subpopulations f4 and f5 (Fig. 5B). In agreement with this and previous

211 reports that C capsids are selectively exported to the cytoplasm [26-29], the frequency of
212 virions in the perinuclear space and cytoplasm in subpopulation f3 was significantly lower
213 than in subpopulations f4 and f5 (Fig. 5C). The frequency of A capsids in subpopulation
214 f3 was comparable to those in subpopulations f4 and f5 (Fig. 5B). The frequencies of each
215 type of nuclear capsid in subpopulations f4 and f5 were similar to those reported
216 previously in wild-type HSV-1-infected HeLa cells [30]. These features of subpopulation
217 f3 were similar to the phenotypes of HSV-1 mutants with defective viral DNA genome
218 cleavage/packaging including those lacking the portal protein UL6, a terminase subunit
219 (UL15, UL33 or UL28) or a minor capsid protein (UL17 or UL32) [31-37].

220 Collectively, these results suggested that the cleavage/packaging of HSV-1 DNA
221 genome was specifically down-regulated in subpopulations below the threshold and that
222 this viral step was a rate-limiting step for progeny virus production.

223 **Expression of a subset of HSV-1 L proteins including all components of viral**
224 **terminase is specifically down-regulated in subpopulations below the threshold for**
225 **progeny virus production.** We compared global HSV-1 L protein abundance in each
226 subpopulation by LC-MS/MS, and there was a strong correlation between the Venus-
227 Us11 fluorescence intensities and relative abundance of each of 49 HSV-1 L proteins (Fig.
228 2). Therefore, we focused on the abundance profiles of the bottom 10 HSV-1 L proteins

with a relatively low correlation (Fig. 6A). The abundance profiles of the bottom 6 HSV-1 L proteins with a relatively low correlation including UL15, UL4, UL33, Us10, UL28 and UL3 differed from those of other HSV-1 L proteins (Fig. 6A and S-Fig. 1B). The abundance of these L proteins in subpopulations f1 to f3 were very low and remained relatively constant, but were increased in subpopulations f4 to f6. These features resembled those observed for the profiles of progeny virus production in these subpopulations 24 h after infection (Fig. 3D). In contrast, the abundances of other HSV-1 L proteins including UL56, UL24, UL37 and UL1 proteins increased in the f1 or f2 subpopulation and continued to increase in the f6 subpopulation. Next, to quantitatively evaluate similarities between profiles of progeny virus production (Fig. 3D) and abundance profiles of HSV-1 L proteins (S-Fig. 1B), a four-parameter logistic regression was used for curve fitting of these profiles 24 h after infection (S-Fig. 6A and B). The x-axis value at which the y-axis value increased by $\log_{10}2$ (2-fold increase in linear scale) from the starting point (x=0) for each curve was defined as the threshold value (TV) (S-Fig. 6A and B), and differences between the TV of progeny virus production and TV of each L protein was calculated (Fig. 6B). UL15, UL4, UL33, Us10, UL28 and UL3 were the top six proteins with the lowest difference, supporting our interpretation that abundance profiles of these six proteins were similar to the profile of progeny virus

production (Fig. 6B). We also applied this analysis to viral mRNA and DNA profiles (S-Fig.4A and B) and found that differences between the TV of progeny virus production and TV of each viral mRNA or DNA were greater than 1.2 (S-Fig. 7), supporting the low similarity between profiles of progeny virus production and profiles of each viral mRNA and DNA described above. Collectively, these results suggested that a particular subset of HSV-1 L proteins including all subunits of viral terminase was specifically down-regulated in subpopulations below the threshold for progeny virus production.

DISCUSSION

This study established a system to fractionate HSV-1-infected cells based on global HSV-1 L protein expression levels and to titrate progeny virus yields in these fractions. This established system enabled us to clarify, for the first time, the direct and quantitative relationship between viral protein expression and progeny virus yields, and the clarified relationship indicated a threshold for HSV-1 L protein expression levels for progeny virus production. Such a threshold has not been reported by classical time course studies of most viruses at the entire population level by analyzing the relationship between viral gene expression and progeny virus yield. In contrast, once the levels of HSV-1 L protein expression exceeded the threshold, they were highly correlated with infectious progeny virus yields as reported by our (Fig. 3B) and other previous studies at the entire population level [4, 6].

The threshold clarified in this study led us to identify the HSV-1 genome DNA cleavage/packaging step was a rate-limiting step for progeny virus production. Supporting this conclusion, MS analysis of the global expression of HSV-1 L proteins at the subpopulation level showed the expression of a subset of HSV-1 L proteins including all components of viral terminase were specifically down-regulated in the subpopulation below the threshold. Conceivably, an anti-viral strategy targeting this bottleneck step for

HSV-1 production might block progeny virus production effectively. HSV-1 genome DNA cleavage/packaging, which is largely mediated by a specific viral enzyme HSV-1 terminase, is essential for viral replication [31, 33, 34, 36], and most targets of antiviral drugs successfully developed to date are viral specific enzymes [38]. Our study at the subpopulation level using this newly established system revealed an ideal target for the development of anti-viral drugs. Notably, the newly established system is simple and widely applicable for studies of the direct relationship between viral gene expression and progeny virus yield of many other DNA and RNA viruses, which might provide specific and conserved insights into mechanisms of progeny virus production in these viruses. It will be particularly interesting to determine whether the rate-limiting step identified in the progeny virus production of HSV-1 is conserved in adenoviruses, which seem to utilize similar DNA genome packaging systems [39].

It has long been recognized that much fewer virions are present in the cytoplasm of HSV-1-infected cells compared with the nucleus [40-42]. Our conclusion that the HSV-1 genome DNA cleavage/packaging step is a rate-limiting step for progeny virus production is in agreement with these observations as well as earlier reports demonstrating C capsids are selectively exported to the cytoplasm [26-29]. The rate-limiting step identified in this study also suggests a sophisticated strategy of efficient progeny virus production by HSV-

1 without accumulating progeny nucleocapsids in the cytoplasm, which enables evasion from cytosolic sensors related to innate immune responses. In the cytoplasm, HSV-1 nucleocapsids are degraded by proteasomes [43], and viral DNAs are likely to be sensed by cytosolic sensors including cGAS, AIM2, DAI, and RNA polymerase III, which promote innate immune responses [44-49]. Here we showed that, in subpopulation f3, which was likely slightly below the threshold, HSV-1 genome DNA replication had already reached a plateau and B capsid formation was easily observed although C capsid formation was barely detectable. In contrast, in subpopulation f4, which was likely slightly over the threshold, C capsids and all types of virions in the perinuclear space and the cytoplasm were evident. These observations suggested that downregulating the HSV-1 DNA cleavage/packaging might promote the accumulation of nucleocapsid components including capsids and viral genome DNAs in the nucleus as well as other viral proteins required for virion maturation at the NMs and in the cytoplasm at a level sufficient for efficient progeny virus production. Once the viral genome is packaged into a capsid, the following steps for virion maturation might immediately proceed without accumulating any excess nucleocapsids in the cytoplasm, decreasing the chance for HSV-1 to be sensed by innate immune responses in the cytoplasm. IFI16 and hnRNPA2B1 sense HSV-1 genome DNA and promote innate immune responses in the nucleus [50-52]. However,

replicated HSV-1 genome DNAs and nucleocapsids appear to accumulate in the nucleus of HSV-1-infected cells [19, 53, 54], suggesting this virus has evolved more effective evasion mechanisms against innate immune responses in the nucleus such that ICP0 counteracts IFI16 [50] and probably, against capsid degradation than those in the cytoplasm.

MATERIALS AND METHODS

Cells and Viruses. HeLa, U2OS, and Vero cells were described previously [20, 55]. Wild-type HSV-1(F) was described previously [56].

Generation of a recombinant virus. Recombinant virus YK410 (rICP47/vUs11) in which ICP47 and Us11 were tagged with TagRFP [57] and VenusA206K [58], respectively, were generated by two rounds of two-step Red-mediated mutagenesis using *Escherichia coli* GS1783 containing pYEbac102Cre [56, 59], a full-length infectious HSV-1(F) clone, pBS-Venus-KanS [20], pFlag-TagRFP-KanS, and the primers listed in Supplementary Table 1. The viruses used in this study were propagated and titrated in Vero cells.

Plasmids. pFlag-TagRFP was constructed by amplifying the TagRFP open reading frame (ORF) to introduce a *Kpn*I site without changing the amino acid sequence by PCR from pTagRFP-N1 [60] and cloning it into pFlag-CMV2 (Sigma). pFlag-TagRFP-KanS, used in the two-step Red-mediated mutagenesis procedure, was constructed by amplifying the domain of pEP-KanS [61] carrying the I-*Sce*I site and the kanamycin resistance gene by PCR from pEP-KanS using the primers 5'-GCGGTACCGTGAACAACCACCACTTCAAAGGATGACGACGATAAGTAGGG-3' and 5'-

GCGGTACCCTCCATGTACAGCTTCATGTCAACCAATTAACCAATTCTGATTA G-3' and cloning it into the *Kpn*I site of pFlag-TagRFP. pGEX-ICP47 was constructed by amplifying the ICP47 ORF by PCR from the HSV-1(F) genome and cloning it into pGEX-4T-1.

Antibodies. Commercial antibodies used in this study included mouse monoclonal antibody to α-tubulin (DM1A; Sigma), and rabbit monoclonal antibodies to GFP (598; MBL) and TagRFP (AB233; Evrogen). Rabbit polyclonal antibodies to US11 were described previously [41]. To generate a rabbit polyclonal antibody to ICP47, a rabbit was immunized, according to the standard protocol at MBL, with GST-ICP47 expressed in *E. coli* and purified as described previously [20]. Serum from the immunized rabbit was used as the anti-ICP47 polyclonal antibody.

Immunoblotting. Immunoblotting was performed as described previously [62].

Flow cytometry. HeLa cells infected with HSV-1(F) or YK410 (rICP47/vUs11) were washed with phosphate buffered saline (PBS) and detached with 0.25% trypsin/EDTA solution (Wako). Then, the cells were suspended in PBS containing 2% FCS, filtered through a 35-μm pore-cell strainer (#352235, Corning) and subjected to FACS analysis with BD FACS Melody (Becton Dickinson). The data were analyzed with

BD FACSChorus (Becton Dickinson) software or FlowJo 10.8.1 software (Becton Dickinson).

Determination of viral titer in cells fractionated by cell sorting. HeLa cells were infected with YK410 (rICP47/vUs11) at an MOI of 5. At the indicated times after infection, cells were detached and suspended as described above. Then, 1.5×10^4 to 3×10^4 cells in the f1 to f6 subpopulations, and the entire cell population (FSC-singlet), were sorted into medium 199 containing 1% FCS by FACS Melody (Becton Dickinson). The sorted cells were freeze-thawed once, sonicated, and virus titers were determined by plaque assay using Vero cells. The average virus titer per single cell was obtained by dividing the obtained virus titer by the number of sorted cells. Data are presented as the PFU per 10^4 cells.

Calculation of the proportion of virus titers in each subpopulation and the virtual titer. PFU_{fi}, which represents the viral titer of each subpopulation fi (i = 1 to 6), was obtained using the following equation:

$$PFU_{fi} = PFU_{fi/cell} \times 10^4 \times PR_{Fi} / 100$$

where $PFU_{fi/cell}$ is the average viral titer per single cell belonging to the fi subpopulation (from Fig. 3D) and PR_{fi} is the proportion (%) of cells in the fi fraction in the entire

population (from Fig. 3E). The virtual titer (VT), which represents the sum of PFU_{fi} (Fig. 3C) was obtained as follows:

$VT = PFU_{f1} + PFU_{f2} + PFU_{f3} + PFU_{f4} + PFU_{f5} + PFU_{f6}$

% of PFU_{Pi}, which represents the proportion of viral titers in the fi subpopulation accounted for in the entire population (Fig. 3F) was obtained using the following equation:

$\% \text{ of } PFU_{fi} = PFU_{fi} / VT \times 100$

LC-MS/MS analysis of cells fractionated by cell sorting. HeLa cells were infected with rICP47/vUs11 at an MOI of 5 for 24 h. Then, cells were detached and suspended as described above. Next, 10^5 cells in the f1 to f6 subpopulation were sorted into PBS by BD FACS Melody (Becton Dickinson), pelleted by centrifugation, and lysed with lysis buffer (0.1 M of Tris-HCl (pH 8.0), 1% SDS). To remove SDS from samples, we used the methanol-chloroform protein precipitation method. Briefly, we added 4 volumes of methanol, 1 volume of chloroform, and 3 volumes of water to the eluted sample and mixed thoroughly. The samples were centrifuged at 15,000 rpm for 10 min, the water phase was carefully removed, and then 4 volumes of methanol were added to the samples. The samples were centrifuged at 15,000 rpm for 10 min, and the supernatant was removed. The pellet was washed once with 100% ice-cold acetone. The precipitated

protein was re-dissolved in guanidine hydrochloride, reduced with TCEP, alkylated with iodoacetamide, and digested with lysyl endopeptidase and trypsin. The resulting digested peptides were analyzed using an Evosep One LC system (EVOSEP) connected to a Q-Exactive HF-X mass spectrometer (Thermo) with a Dream spray tip (AMR) and a 15 cm × 150 μm column packed with 1.9-μm C18-beads (Evosep). The mobile phases were comprised of 0.1% FA as solution A and 0.1% FA/99.9% ACN as solution B. The analysis was performed in the data-dependent acquisition mode, where the top 25 recorded mass spectrometry spectra between 380 and 1500 m/z were selected. Survey scans were acquired at a resolution of 60,000 at m/z 200, and the tandem mass spectrometry (MS/MS) resolution was set to 15,000 at m/z 200. All MS/MS spectra were searched against the protein sequences of the HSV protein database and human Swiss-Prot database using Proteome Discoverer 2.2 (Thermo) with the SEQUEST search engine, and the result of HSV proteins was extracted. The false discovery rate (FDR) was set to 1% on peptide spectrum match (PSM).

Data processing of LC-MS/MS data. Normalization was performed on quantitative values using the method built into the Discoverer 2.2 software. Briefly, the Total Peptide Amount mode was used to normalize between samples, and the On All Average mode was used to normalize between identified proteins. The subsequent

analysis was performed using only the extracted data for HSV proteins. The normalization method in each mode was as follows. The Total Peptide Amount mode sums the peptide group abundances for each sample and determines the maximum sum for all files. The normalization factor is the factor of the sum of the samples and the maximum sum in all files. The On All Average mode aggregates all the abundance or normalized abundance values per sample and scales the abundance values of each sample so that the average of all samples is 100. When a peptide was not detected in all replicates of each subpopulation, the protein was considered undetectable in that subpopulation. When a peptide was not detected in a replicate of each subpopulation, the missing value was complemented with the mean value of abundances in replicates where the peptide was detected. The relative abundance of each HSV-1 L protein was calculated relative to the subpopulation with the lowest mean abundance for 4 replicates as 1.

RNA-sequencing in cells fractionated by cell sorting. HeLa cells were infected with YK410 (rICP47/vUs11) at an MOI of 5 for 24 h. Then, cells were detached and suspended as described above. Next, 5×10^5 cells in the f1 to f6 subpopulations were sorted into PBS by BD FACS Melody (Becton Dickinson). After centrifugation, total RNA from fractionated cells was isolated with a High Pure RNA Isolation kit (Roche). (i) Each cDNA was generated using a Clontech SMART-Seq HT Kit (Takara Clontech,

Mountain View, CA, USA), and each library was prepared using a Nextera XT DNA Library Prep Kit (Illumina, San Diego, USA). Sequencing was performed on the DNBSEQ-G400 platform in the 100+100-base paired-end mode. (ii) Generated reads were a mixture of human reads and HSV-1 reads. For human data, generated reads were mapped to the human (hg19) reference genome using TopHat v2.1.1 combined with Bowtie2 ver. 2.2.8 and SAMtools ver. 0.1.18. For HSV-1, generated reads were mapped to the HSV-1 (GenBank: GU734771.1) reference genome using HISAT2 v2.1.0. (iii) The quantification to obtain the read counts of each gene from HSV-1 was performed using featureCounts of subread-2.0.0 with option -M --fraction. With the length data of each gene (another output of the featureCounts), fragments per kilobase of exon per million mapped fragments (FPKMs) were calculated according to the definition. The FPKM of HSV-1 genes was multiplied by (total number of mapped reads of the HSV-1 genome)/{(total number of mapped reads of the human genome) + (total number of mapped reads of the HSV-1 genome)}, normalized by the amount relative to the value of the f1 fraction.

Quantification of HSV-1 DNA in cells fractionated by cell sorting. HeLa cells were infected with YK410 (rICP47/vUs11) at an MOI of 5 for 24 h. Then, cells were detached and suspended as described above. Next, 5×10^4 cells in the f1 to f6

subpopulations were sorted into PBS by BD FACS Melody (Becton Dickinson). After centrifugation, total DNA from fractionated cells was isolated with NucleoSpin Tissue XS (TAKARA) according to the manufacturer's instructions. The amount of HSV-1 DNA was quantified using the Universal Probe Library (Roche) with TaqMan Master (Roche) and the LightCycler 96 System (Roche) according to the manufacturer's instructions. Primers and probes were designed using probe finder software within the region encoding ICP27 in the HSV-1 genome, and within the region encoding 18S rRNA in the human genome. The primer and probe sequences for ICP27 (for HSV-1 DNA) were 5′-TCCGACAGCGATCTGGAC-3′, 5′-TCCGACGAGGAACACTCC-3′, and Universal ProbeLibrary probe 56, and for 18S rRNA (for human DNA) the sequences were 5′-GCAATTATTCCCCATGAACG-3′, 5′-GGGACTTAATCAACGCAAGC-3′, and Universal ProbeLibrary probe 48. The ΔCt was calculated by subtracting the Ct value of HSV-1 DNA by the Ct value of human DNA. The relative amount of HSV-1 DNA to human DNA ($2^{-\Delta Ct}$) was normalized relative to the value of the f1 subpopulation.

Electron microscopic analysis of cells fractionated by cell sorting. HeLa cells were infected with YK410 (rICP47/vUs11) at an MOI of 5 for 24 h. Then, cells were detached and suspended as described above. Next, 5×10^5 to 1×10^6 cells in the f2 to f5 subpopulations were sorted by BD FACS Melody (Becton Dickinson). After

centrifugation, the pelleted cells were examined by ultrathin-section electron microscopy as described previously [63] except using JEM-1400 Flash microscope (JEOL).

Statistical analysis. The unpaired Student's *t*-test was used to compare two groups. One-way ANOVA followed by the Tukey multiple comparisons test, or Mann-Whitney *U*-test followed by Bonferroni correction were used for multiple comparisons. A P-value < 0.05 was considered statistically significant. Pearson correlation coefficients (r) and p-values were calculated on log10 transformed data. GraphPad Prism 9 (GraphPad Software) was used to perform statistical analyses.

Classification of HSV-1 genes. HSV-1 genes were classified into IE, E, and L genes as described previously [19].

Curve fitting. To describe the profiles of progeny virus and abundance profiles of HSV-1 L proteins, DNA, and mRNA, we mainly used the following mathematical model developed by dose response modeling [64].

$$f(x) = c + \frac{d - c}{1 + \exp\big(b(x - a)\big)} \qquad (1)$$

The variable $f(x)$ is the profiles of progeny viruses or abundance profiles of HSV-1 L proteins, DNA, or mRNA. The parameter a is the inflection point of the curve for this model, that is, the point where a change in acceleration in the curve occurs. The parameter

b is a slope parameter and the parameters c and d are the lower and upper horizontal asymptotes or limits, respectively.

Fitting was performed by drc package in R, which estimates the parameters with nonlinear least squares under the assumption of normally distributed response values [65].

ACKNOWLEDGEMENTS

We thank Risa Abe, Tohru Ikegami and Yui Muto for their excellent technical assistance. We acknowledge the NGS core facility of the Genome Information Research Center at the Research Institute for Microbial Diseases of Osaka University for the support in RNA sequencing and data analysis. This study was supported by Grants for Scientific Research and Grant-in-Aid for Scientific Research (S) (20H05692) from the Japan Society for the Promotion of Science (JSPS), grants for Scientific Research on Innovative Areas (21H00338, 21H00417, 22H04803) and a grant for Transformative Research Areas (22H05584) from the Ministry of Education, Culture, Science, Sports and Technology of Japan, PRESTO (JPMJPR22R5), SPRING (JPMJSP2018), MIRAI (JPMJMI22G1) and Moonshot R&D (JPMJM2021, JPMJMS2025) from Japan Science and Technology Agency (JST), grants (JP20wm0125002, JP22fk0108640, JP22gm1610008, JP223fa627001) from the Japan Agency for Medical Research and Development (AMED), grants from the International Joint Research Project of the Institute of Medical Science, the University of Tokyo, and grants from the Takeda Science Foundation, the Uehara Memorial Foundation and the Mitsubishi Foundation.

FIGURE LEGENDS

Fig. 1. Characterization of the reporter HSV-1 rICP47/vUs11 generated in this study. (A) Schematic diagram of the genome structure of wild-type HSV-1(F) and rICP47/vUs11. Line 1, wild-type HSV-1(F) genome; line 2, domains of the Us11 and ICP47 coding regions. The positions of insertion of TagRFP and Venus are indicated. (B) HeLa cells mock-infected or infected for 24 h with wild-type HSV-1(F) or rICP47/vUs11 at an MOI of 5 were lysed and analyzed by immunoblotting with the indicated antibodies. (C) HeLa cells were infected at an MOI of 5 with wild-type HSV-1(F) or rICP47/vUs11. Each cell culture supernatant plus the infected cells were harvested at the indicated times post infection, and progeny viruses were assayed on Vero cells. (D) HeLa cells infected for 24 h with wild-type HSV-1(F) or rICP47/vUs11 at an MOI of 5 were analyzed by flow cytometry. (E) Quantitative bar graph of the proportion of cells in the TagRFP/Venus (+/+), TagRFP/Venus (+/-), TagRFP/Venus (-/+), and TagRFP/Venus (-/-) subpopulations shown in (D). (F) CV values for TagRFP-ICP47 and Venus-Us11 shown in (D). The data are representative of three independent experiments (B and D). Each value is the mean ± standard error of the results of four (C) or three (E and F) independent experiments. Statistical analysis was performed by unpaired Student's *t*-test. ns, not significant (C and F).

Fig. 2. Abundance of HSV-1 L proteins in each subpopulation of rICP47/vUs11-infected cells. (A) HeLa cells were infected for 24 h with rICP47/vUs11 at an MOI of 5 and sorted into six subpopulations (f1 to f6) by cell sorting as shown in S. Fig. 1A and each subpopulation was analyzed by LC-MS/MS. The heatmap of log10 (relative abundance) of 49 HSV-1 L proteins in each subpopulation is shown. X: not detectable. Peptides of UL4 were not detectable in subpopulations f1 and f2 and those of UL33 were not detectable in subpopulation f2. (B) Heatmap of the Pearson correlation coefficient between $\log_{10}$ (MFI of Venus) of each subpopulation and $\log_{10}$ (relative abundance) of each HSV-1 L protein. For UL4 and UL33, when peptides were not detected in the subpopulations above, Pearson correlation coefficients were calculated by completing missing values with 0. P-values for the correlation coefficient of all HSV-1 L proteins shown in B were < 0.05.

Fig. 3. Quantitative analysis of a relationship between the expression levels of HSV-1 L proteins and progeny virus yields. (A to H) HeLa cells were infected with rICP47/vUs11 at an MOI of 5, analyzed by flow cytometry, and sorted into an entire cell population (FSC singlet) or f1 to f6 subpopulations by cell sorting at the indicated times after infection as shown in S. Fig.2. Sorted cells were sonicated and virus titers were

determined by plaque assay using Vero cells. (A) Kinetics of mean fluorescent intensity (MFI) of Venus and progeny virus titers of the entire population. (B) Scatter plot of $\log_{10}$(relative MFI of Venus) vs $\log_{10}$(PFU/10^4 cells) from panel A. (C) Kinetics of progeny virus titers of the entire population from panel A (actual) and sum of the virus titers produced by each subpopulation (virtual). The calculation method for virtual titers is described in the Materials and methods. (D) Scatter plots of $\log_{10}$(relative MFI of Venus) vs $\log_{10}$(PFU/10^4 cells) of the indicated subpopulation separated by time after infection. (E) Proportion of cells in the indicated subpopulation account for the entire cell population at the indicated times after infection. (F) Proportion of virus titers produced by the f1 to f6 subpopulations account for virus titers produced by the entire population at the indicated times after infection. (G) Scatter plot of $\log_{10}$(relative MFI of Venus) vs $\log_{10}$(PFU/10^4 cells) of f1 to f3 (left), or f4 to f6 (right) subpopulations. The data are from panel D. (H) Progeny virus titers of the indicated subpopulations at the indicated times after infection. The data are from panel D. Each value is the mean ± standard error (A, C, D, E, F, and H) or mean (B and G) of the results of three independent experiments. Statistical analysis was performed by unpaired Student's *t*-test. ns, not significant (C). Solid and dashed lines indicate 1 PFU/cell and 0.1 PFU/cell, respectively (D and H).

Fig. 4. Electron microscopic analysis of cells in the f2 to f5 subpopulations. (A and B) HeLa cells were infected with rICP47/vUs11 at an MOI of 5 and sorted into four subpopulations (f2 to f5) by cell sorting 24 h after infection. Sorted cells were fixed, embedded, sectioned, stained, and examined by electron microscopy. (A) A transmission electron microscopy image of cells in the f2 to f5 subpopulations. n, nucleus; c, cytoplasm. Scale bars = 500 nm. (B) The numbers of nuclear virions, enveloped virions in the perinuclear space, naked capsids in the cytoplasm, and enveloped virions in the cytoplasm of 10 cells in the f2 to f5 subpopulations were quantitated. The horizontal bars indicate the means.

Fig. 5. Frequencies of A, B, and C capsids in the nucleus of cells in the f2 to f5 subpopulations. (A) The numbers of A, B, and C capsids in the nucleus of 11 cells analyzed in Fig. 4 in the f2 to f5 subpopulations were quantitated. The horizontal bars indicate the means ± standard errors. Proportions of A, B, and C capsids to nuclear capsids (B), or virions in the perinuclear space and cytoplasm (C) of cells with more than two nuclear capsids (f3, n = 9; f4, n = 11; f5, n = 11). Data are presented as the median ± interquartile range (IQR). Statistical analysis was performed by the Mann-Whitney *U*-test, and P-values were adjusted by Bonferroni correction. ns, not significant.

Fig. 6. Abundance of 10 HSV-1 L proteins in each subpopulation of rICP47/vUs11 infected cells. (A) Scatter plots of $\log_{10}$(relative MFI of Venus) vs $\log_{10}$(relative abundance) of L proteins (from S. Fig. 1B) of the bottom 10 HSV-1 L proteins with relatively low correlation coefficients between fluorescence intensity of Venus and their abundance (from Fig. 2B). Plots of terminase subunits are marked with magenta squares. (B) Difference between the TV of progeny virus production (TVpv) (from S. Fig 6A) and TV of 40 L proteins (TVlp) (from S. Fig. 6B). Data of terminase subunits are shown in magenta.

Supplementary Fig. 1. Abundance of HSV-1 L proteins in each subpopulation of rICP47/vUs11 infected cells. (A) Gating strategy for the LC-MS/MS analysis of HeLa cells infected with rICP47/vUs11 at an MOI of 5 for 24 h. (B) Scatter plots of $\log_{10}$(relative MFI of Venus) vs $\log_{10}$(relative abundances) of the 49 indicated HSV-1 L proteins. Each value is the mean ± standard error of the results of four technical replicates.

Supplementary Fig. 2. Quantitative analysis of a relationship between the expression levels of HSV-1 L proteins and progeny virus yields. Gating strategy for the experiments shown in Fig. 3.

Supplementary Fig. 3. Quantitative analysis of the relationship between the expression levels of HSV-1 L proteins and progeny virus yields under different experimental conditions. (A to D) HeLa cells infected with rICP47/vUs11 at the indicated MOI for 24 h, were sorted into f1 to f6 subpopulations (A), sonicated and virus titers were determined by plaque assay using Vero cells. (B) Scatter plot of $\log_{10}$(relative MFI of Venus) vs $\log_{10}$(PFU/10^4 cells). (C) Proportion of cells in the indicated subpopulations account for the entire cell population at the indicated MOIs. (D) Proportion of virus titers produced by the f1 to f6 subpopulations account for virus titers produced by the entire population at the indicated times after infection. Vero (E to H), or

U2OS (I to L) cells infected with rICP47/vUs11 at an MOI of 1 (E to H) or 2.5 (I to L) for 12 h, were sorted into f1 to f6 subpopulations (E and I), sonicated, and virus titers were determined by plaque assay using Vero cells. (F and J) Scatter plots of $\log_{10}$(relative MFI of Venus) vs $\log_{10}$(PFU/10^4 cells) of each subpopulation. (G and K) Proportion of cells in the f1 to f6 subpopulations account for the entire cell population. (H and L) Proportion of virus titers produced by each subpopulation account for the virus titers produced by the entire cell population. The data are representative of three independent experiments (A, E, and I). Each value is the mean ± standard error of the results of three independent experiments (B, C, D, F, G, H, J, K, and L). Solid and dashed lines indicate 1 PFU/cell and 0.1 PFU/cell, respectively (B, F and J).

Supplementary Fig. 4. Amount of HSV-1 DNA and mRNA in the f1 to f6 subpopulations. (A and B) HeLa cells were infected for 24 h with rICP47/vUs11 at an MOI of 5 and sorted into six subpopulations (f1 to f6) by cell sorting. Relative amounts of HSV-1 DNA (A) and mRNA (B) of selected genes in each subpopulation were analyzed by quantitative PCR or RNA-seq, respectively. Scatter plot of $\log_{10}$(relative MFI of Venus) vs $\log_{10}$(relative amount of HSV-1 DNA) (A), or scatter plots of $\log_{10}$(relative MFI of Venus) vs $\log_{10}$(relative FPKM) of the indicated HSV-1 genes (B) are shown.

Each value is the mean ± standard error of the results of three biologically independent samples.

Supplementary Fig. 5. Frequency of A, B, and C capsids in the nucleus of cells in f2 to f5 subpopulations. A transmission electron microscopy image of cells in the f2 to f5 subpopulations. n, nucleus; c, cytoplasm from the experiment in Fig. 4. Type A capsids are marked in green, B capsids in blue, and C capsids in red. Scale bars = 500 nm.

Supplementary Fig. 6. Curve fitting to profiles of progeny virus production and abundance profiles of HSV-1 L proteins. (A) Scatter plot of $\log_{10}$(relative MFI of Venus) vs $\log_{10}$(PFU/10^4 cells) 24 h after infection (from Fig. 3D), and (B) scatter plots of $\log_{10}$(relative MFI of Venus) vs $\log_{10}$(relative abundances) of the 49 indicated HSV-1 L proteins (from S-Fig. 1B) were fitted to a four-parameter logistic regression curve. TVs are the x-axis value at which the y-axis value increases by $\log_{10}2$ (2-fold increase in linear scale) from the starting point (x = 0) for each curve. The grey regions correspond to 95% confidence intervals.

Supplementary Fig. 7. Curve fitting to abundance profiles of HSV-1 DNA and mRNA. (A) Scatter plot of $\log_{10}$(relative MFI of Venus) vs $\log_{10}$(relative amount of HSV-1 DNA), or scatter plots of $\log_{10}$(relative MFI of Venus) vs $\log_{10}$(relative FPKM) of the indicated HSV-1 genes were fitted to a four-parameter logistic regression curve. TVs are the x-axis value at which the y-axis value increases by $\log_{10}2$ (2-fold increase in linear scale) from the starting point (x = 0) for each curve. The grey regions correspond to 95% confidence intervals. (B) Difference between the TV of progeny virus production (TVpv) (from S. Fig 6A) and TV of HSV-1 DNA (TVdn) (from S. Fig 7A) or (C) viral mRNA (TVmr) (from S. Fig 7A).

REFERENCES

1. Whelan, S. Viral Replication Strategies, in *Fields virology*, Edn. 6th. (eds. D.M. Knipe *et al.*) 105-126 (Lippincott-Williams & Wilkins, Philadelphia, PA; 2013).
2. Brown, D.M. *et al.* Cell-dependent role for the poliovirus 3' noncoding region in positive-strand RNA synthesis. *J Virol* **78**, 1344-1351 (2004).
3. Kim, D. *et al.* A high-resolution temporal atlas of the SARS-CoV-2 translatome and transcriptome. *Nat Commun* **12**, 5120 (2021).
4. Lloyd, M.G. *et al.* Development of Robust Varicella Zoster Virus Luciferase Reporter Viruses for In Vivo Monitoring of Virus Growth and Its Antiviral Inhibition in Culture, Skin, and Humanized Mice. *Viruses* **14** (2022).
5. Ouwendijk, W.J.D. *et al.* Analysis of Virus and Host Proteomes During Productive HSV-1 and VZV Infection in Human Epithelial Cells. *Front Microbiol* **11**, 1179 (2020).
6. Tamura, T. *et al.* Characterization of Recombinant Flaviviridae Viruses Possessing a Small Reporter Tag. *J Virol* **92** (2018).
7. Delbruck, M. The burst size distribution in the growth of bacterial viruses (bacteriophages). *J Bacteriol* **50**, 131-135 (1945).
8. Zhu, Y., Yongky, A. & Yin, J. Growth of an RNA virus in single cells reveals a broad fitness distribution. *Virology* **385**, 39-46 (2009).
9. Timm, A. & Yin, J. Kinetics of virus production from single cells. *Virology* **424**, 11-17 (2012).
10. Schulte, M.B. & Andino, R. Single-cell analysis uncovers extensive biological noise in poliovirus replication. *J Virol* **88**, 6205-6212 (2014).

662 11. Combe, M., Garijo, R., Geller, R., Cuevas, J.M. & Sanjuan, R. Single-Cell Analysis of
663 RNA Virus Infection Identifies Multiple Genetically Diverse Viral Genomes within
664 Single Infectious Units. *Cell Host Microbe* **18**, 424-432 (2015).
665 12. Heldt, F.S., Kupke, S.Y., Dorl, S., Reichl, U. & Frensing, T. Single-cell analysis and
666 stochastic modelling unveil large cell-to-cell variability in influenza A virus infection.
667 *Nat Commun* **6**, 8938 (2015).
668 13. Wildy, P., Stoker, M.G.P. & Ross, R.W. Release of Herpes Virus from Solitary HeLa
669 Cells. *Journal of General Microbiology* **20**, 105-112 (1959).
670 14. Bacsik, D.J. *et al.* Influenza virus transcription and progeny production are poorly
671 correlated in single cells. *bioRxiv*, 2022.2008.2030.505828 (2023).
672 15. Drayman, N., Patel, P., Vistain, L. & Tay, S. HSV-1 single-cell analysis reveals the
673 activation of anti-viral and developmental programs in distinct sub-populations. *Elife*
674 **8** (2019).
675 16. Ku, C. *et al.* A single-cell view on alga-virus interactions reveals sequential
676 transcriptional programs and infection states. *Sci Adv* **6**, eaba4137 (2020).
677 17. Suomalainen, M. & Greber, U.F. Virus Infection Variability by Single-Cell Profiling.
678 *Viruses* **13** (2021).
679 18. Knipe, D.M. *et al.* Herpes Simplex Viruses: Pathogenesis and Clinical Insights, in
680 *Fields virology*, Vol. 2, Edn. 7th. (eds. P.M. Howley *et al.*) 297-323 (Lippincott-
681 Williams & Wilkins, Philadelphia, PA; 2022).

682 19. Roizman, B., Knipe, D.M. & Whitley, R.J. Herpes simplex viruses, in *Fields virology*,
683 Edn. 6th. (eds. D.M. Knipe *et al.*) 1823-1897 (Lippincott-Williams & Wilkins,
684 Philadelphia, PA; 2013).
685 20. Kato, A. *et al.* Identification of a herpes simplex virus 1 gene encoding neurovirulence
686 factor by chemical proteomics. *Nat Commun* **11**, 4894 (2020).
687 21. Whisnant, A.W. *et al.* Integrative functional genomics decodes herpes simplex virus
688 1. *Nat Commun* **11**, 2038 (2020).
689 22. Cohen, E.M., Avital, N., Shamay, M. & Kobiler, O. Abortive herpes simplex virus
690 infection of nonneuronal cells results in quiescent viral genomes that can reactivate.
691 *Proc Natl Acad Sci U S A* **117**, 635-640 (2020).
692 23. Cardone, G., Heymann, J.B., Cheng, N., Trus, B.L. & Steven, A.C. Procapsid
693 assembly, maturation, nuclear exit: dynamic steps in the production of infectious
694 herpesvirions. *Adv Exp Med Biol* **726**, 423-439 (2012).
695 24. Homa, F.L. Capsid assembly and DNA packaging in herpes simplex virus. *Reviews*
696 *in medical virology* **7**, 107-122 (1997).
697 25. Baines, J.D. Herpes simplex virus capsid assembly and DNA packaging: a present
698 and future antiviral drug target. *Trends Microbiol* **19**, 606-613 (2011).
699 26. Takeshima, K. *et al.* Identification of the Capsid Binding Site in the Herpes Simplex
700 Virus 1 Nuclear Egress Complex and Its Role in Viral Primary Envelopment and
701 Replication. *J Virol* **93** (2019).

702 27. Yang, K. & Baines, J.D. Selection of HSV capsids for envelopment involves
703 interaction between capsid surface components pUL31, pUL17, and pUL25. *Proc*
704 *Natl Acad Sci U S A* **108**, 14276-14281 (2011).
705 28. Yang, K., Wills, E., Lim, H.Y., Zhou, Z.H. & Baines, J.D. Association of herpes
706 simplex virus pUL31 with capsid vertices and components of the capsid vertex-
707 specific complex. *J Virol* **88**, 3815-3825 (2014).
708 29. Johnson, D.C. & Baines, J.D. Herpesviruses remodel host membranes for virus egress.
709 *Nat Rev Microbiol* **9**, 382-394 (2011).
710 30. Khadivjam, B., Bonneil, E., Thibault, P. & Lippe, R. RNA helicase DDX3X modulates
711 herpes simplex virus 1 nuclear egress. *Commun Biol* **6**, 134 (2023).
712 31. Heming, J.D., Conway, J.F. & Homa, F.L. Herpesvirus Capsid Assembly and DNA
713 Packaging. *Adv Anat Embryol Cell Biol* **223**, 119-142 (2017).
714 32. Patel, A.H., Rixon, F.J., Cunningham, C. & Davison, A.J. Isolation and
715 characterization of herpes simplex virus type 1 mutants defective in the UL6 gene.
716 *Virology* **217**, 111-123 (1996).
717 33. Baines, J.D., Cunningham, C., Nalwanga, D. & Davison, A. The U(L)15 gene of
718 herpes simplex virus type 1 contains within its second exon a novel open reading
719 frame that is translated in frame with the U(L)15 gene product. *J Virol* **71**, 2666-2673
720 (1997).
721 34. Yang, K., Dang, X. & Baines, J.D. A Domain of Herpes Simplex Virus pU(L)33
722 Required To Release Monomeric Viral Genomes from Cleaved Concatemeric DNA. *J*
723 *Virol* **91** (2017).

724 35. Salmon, B., Cunningham, C., Davison, A.J., Harris, W.J. & Baines, J.D. The herpes
725 simplex virus type 1 U(L)17 gene encodes virion tegument proteins that are required
726 for cleavage and packaging of viral DNA. *J Virol* **72**, 3779-3788 (1998).
727 36. Tengelsen, L.A., Pederson, N.E., Shaver, P.R., Wathen, M.W. & Homa, F.L. Herpes
728 simplex virus type 1 DNA cleavage and encapsidation require the product of the
729 UL28 gene: isolation and characterization of two UL28 deletion mutants. *J Virol* **67**,
730 3470-3480 (1993).
731 37. Lamberti, C. & Weller, S.K. The herpes simplex virus type 1 cleavage/packaging
732 protein, UL32, is involved in efficient localization of capsids to replication
733 compartments. *J Virol* **72**, 2463-2473 (1998).
734 38. Tompa, D.R., Immanuel, A., Srikanth, S. & Kadhirvel, S. Trends and strategies to
735 combat viral infections: A review on FDA approved antiviral drugs. *Int J Biol*
736 *Macromol* **172**, 524-541 (2021).
737 39. Ahi, Y.S. & Mittal, S.K. Components of Adenovirus Genome Packaging. *Front*
738 *Microbiol* **7**, 1503 (2016).
739 40. Lymberopoulos, M.H., Bourget, A., Ben Abdeljelil, N. & Pearson, A. Involvement of
740 the UL24 protein in herpes simplex virus 1-induced dispersal of B23 and in nuclear
741 egress. *Virology* **412**, 341-348 (2011).
742 41. Takeshima, K., Maruzuru, Y., Koyanagi, N., Kato, A. & Kawaguchi, Y. Redundant
743 and Specific Roles of A-Type Lamins and Lamin B Receptor in Herpes Simplex Virus
744 1 Infection. *J Virol* **96**, e0142922 (2022).

745 42. Hutchinson, L. & Johnson, D.C. Herpes simplex virus glycoprotein K promotes egress
746 of virus particles. *J Virol* **69**, 5401-5413 (1995).
747 43. Horan, K.A. *et al.* Proteasomal degradation of herpes simplex virus capsids in
748 macrophages releases DNA to the cytosol for recognition by DNA sensors. *J Immunol*
749 **190**, 2311-2319 (2013).
750 44. Chiu, Y.H., Macmillan, J.B. & Chen, Z.J. RNA polymerase III detects cytosolic DNA
751 and induces type I interferons through the RIG-I pathway. *Cell* **138**, 576-591 (2009).
752 45. Takaoka, A. *et al.* DAI (DLM-1/ZBP1) is a cytosolic DNA sensor and an activator of
753 innate immune response. *Nature* **448**, 501-505 (2007).
754 46. Sun, L., Wu, J., Du, F., Chen, X. & Chen, Z.J. Cyclic GMP-AMP synthase is a cytosolic
755 DNA sensor that activates the type I interferon pathway. *Science* **339**, 786-791 (2013).
756 47. Li, X.D. *et al.* Pivotal roles of cGAS-cGAMP signaling in antiviral defense and
757 immune adjuvant effects. *Science* **341**, 1390-1394 (2013).
758 48. Maruzuru, Y. *et al.* Herpes Simplex Virus 1 VP22 Inhibits AIM2-Dependent
759 Inflammasome Activation to Enable Efficient Viral Replication. *Cell Host Microbe* **23**,
760 254-265 e257 (2018).
761 49. Lee, S. *et al.* AIM2 forms a complex with pyrin and ZBP1 to drive PANoptosis and
762 host defence. *Nature* **597**, 415-419 (2021).
763 50. Orzalli, M.H., DeLuca, N.A. & Knipe, D.M. Nuclear IFI16 induction of IRF-3
764 signaling during herpesviral infection and degradation of IFI16 by the viral ICP0
765 protein. *Proc Natl Acad Sci U S A* **109**, E3008-3017 (2012).

766 51. Li, T., Diner, B.A., Chen, J. & Cristea, I.M. Acetylation modulates cellular
767 distribution and DNA sensing ability of interferon-inducible protein IFI16. *Proc Natl*
768 *Acad Sci U S A* **109**, 10558-10563 (2012).
769 52. Wang, L., Wen, M. & Cao, X. Nuclear hnRNPA2B1 initiates and amplifies the innate
770 immune response to DNA viruses. *Science* **365** (2019).
771 53. Morgan, C., Ellison, S.A., Rose, H.M. & Moore, D.H. Structure and development of
772 viruses as observed in the electron microscope. I. Herpes simplex virus. *J Exp Med*
773 **100**, 195-202 (1954).
774 54. de Bruyn Kops, A. & Knipe, D.M. Formation of DNA replication structures in herpes
775 virus-infected cells requires a viral DNA binding protein. *Cell* **55**, 857-868 (1988).
776 55. Sato, Y. *et al.* Cellular Transcriptional Coactivator RanBP10 and Herpes Simplex
777 Virus 1 ICP0 Interact and Synergistically Promote Viral Gene Expression and
778 Replication. *J Virol* **90**, 3173-3186 (2016).
779 56. Tanaka, M., Kagawa, H., Yamanashi, Y., Sata, T. & Kawaguchi, Y. Construction of
780 an excisable bacterial artificial chromosome containing a full-length infectious clone
781 of herpes simplex virus type 1: viruses reconstituted from the clone exhibit wild-type
782 properties in vitro and in vivo. *J Virol* **77**, 1382-1391 (2003).
783 57. Merzlyak, E.M. *et al.* Bright monomeric red fluorescent protein with an extended
784 fluorescence lifetime. *Nat Methods* **4**, 555-557 (2007).
785 58. Kremers, G.J., Goedhart, J., van Munster, E.B. & Gadella, T.W., Jr. Cyan and yellow
786 super fluorescent proteins with improved brightness, protein folding, and FRET
787 Forster radius. *Biochemistry* **45**, 6570-6580 (2006).

788 59. Kato, A. *et al.* Roles of the Phosphorylation of Herpes Simplex Virus 1 UL51 at a
789 Specific Site in Viral Replication and Pathogenicity. *J Virol* **92** (2018).
790 60. Arii, J. *et al.* Role of the Arginine Cluster in the Disordered Domain of Herpes
791 Simplex Virus 1 UL34 for the Recruitment of ESCRT-III for Viral Primary
792 Envelopment. *J Virol* **96**, e0170421 (2022).
793 61. Tischer, B.K., von Einem, J., Kaufer, B. & Osterrieder, N. Two-step red-mediated
794 recombination for versatile high-efficiency markerless DNA manipulation in
795 Escherichia coli. *Biotechniques* **40**, 191-197 (2006).
796 62. Kawaguchi, Y., Van Sant, C. & Roizman, B. Herpes simplex virus 1 alpha regulatory
797 protein ICP0 interacts with and stabilizes the cell cycle regulator cyclin D3. *J Virol*
798 **71**, 7328-7336 (1997).
799 63. Sagou, K., Imai, T., Sagara, H., Uema, M. & Kawaguchi, Y. Regulation of the catalytic
800 activity of herpes simplex virus 1 protein kinase Us3 by autophosphorylation and its
801 role in pathogenesis. *J Virol* **83**, 5773-5783 (2009).
802 64. Ritz, C. Toward a unified approach to dose-response modeling in ecotoxicology.
803 *Environmental Toxicology and Chemistry* **29**, 220-229 (2010).
804 65. Ritz, C., Baty, F., Streibig, J.C. & Gerhard, D. Dose-Response Analysis Using R.
805 *PLOS ONE* **10**, e0146021 (2015).

806

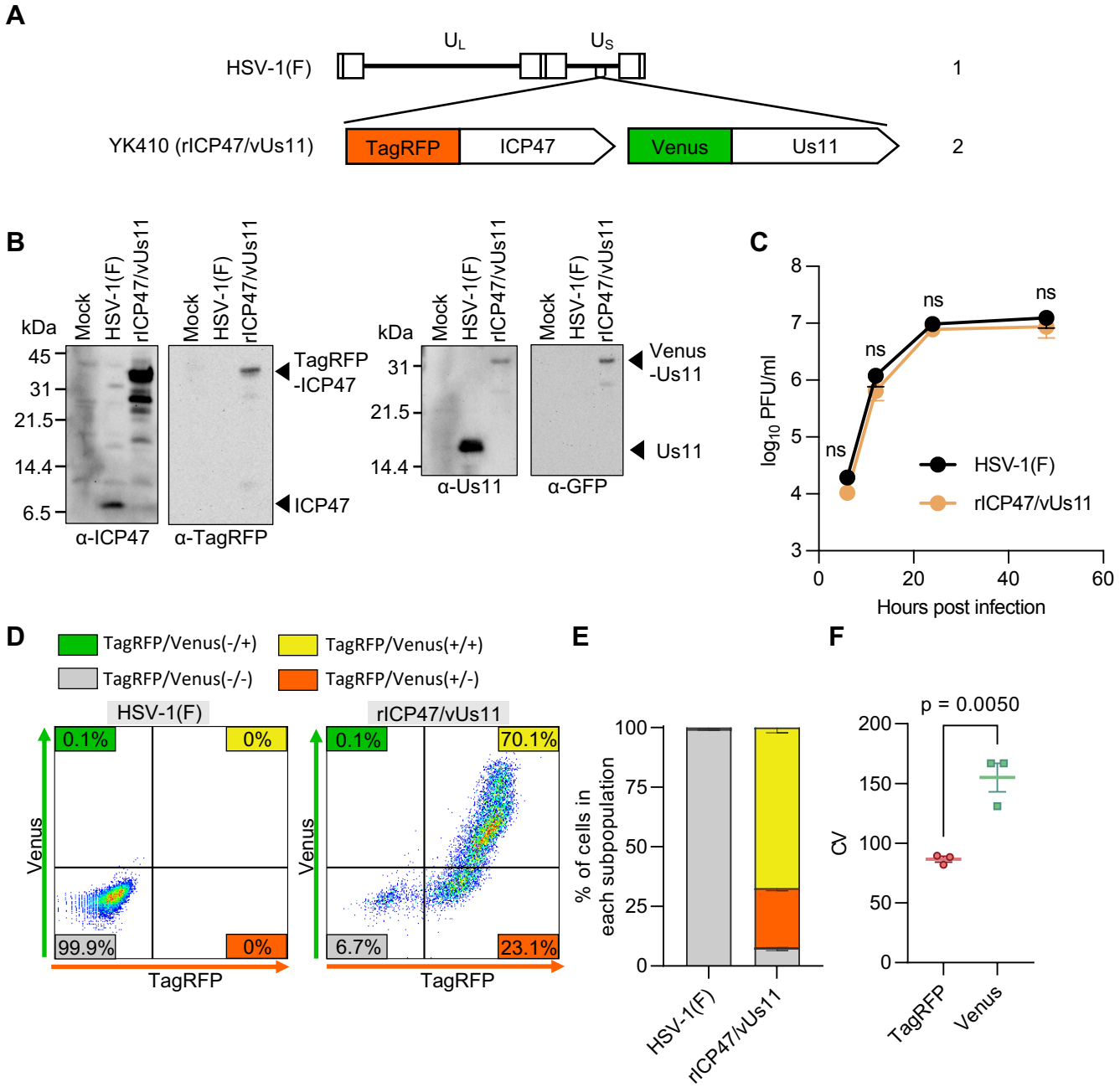

Fig. 1. Characterization of the reporter HSV-1 rICP47/vUs11 generated in this study. (A) Schematic diagram of the genome structure of wild-type HSV-1(F) and rICP47/vUs11. Line 1, wild-type HSV-1(F) genome; line 2, domains of the Us11 and ICP47 coding regions. The positions of insertion of TagRFP and Venus are indicated. (B) HeLa cells mock-infected or infected for 24 h with wild-type HSV-1(F) or rICP47/vUs11 at an MOI of 5 were lysed and analyzed by immunoblotting with the indicated antibodies. (C) HeLa cells were infected at an MOI of 5 with wild-type HSV-1(F) or rICP47/vUs11. Each cell culture supernatant plus the infected cells were harvested at the indicated times post infection, and progeny viruses were assayed on Vero cells. (D) HeLa cells infected for 24 h with wild-type HSV-1(F) or rICP47/vUs11 at an MOI of 5 were analyzed by flow cytometry. (E) Quantitative bar graph of the proportion of cells in the TagRFP/Venus (+/+), TagRFP/Venus (+/-), TagRFP/Venus (-/+), and TagRFP/Venus (-/-) subpopulations shown in (D). (F) CV values for TagRFP-ICP47 and Venus-Us11 shown in (D). The data are representative of three independent experiments (B and D). Each value is the mean ± standard error of the results of four (C) or three (E and F) independent experiments. Statistical analysis was performed by unpaired Student's *t*-test. ns, not significant (C and F).

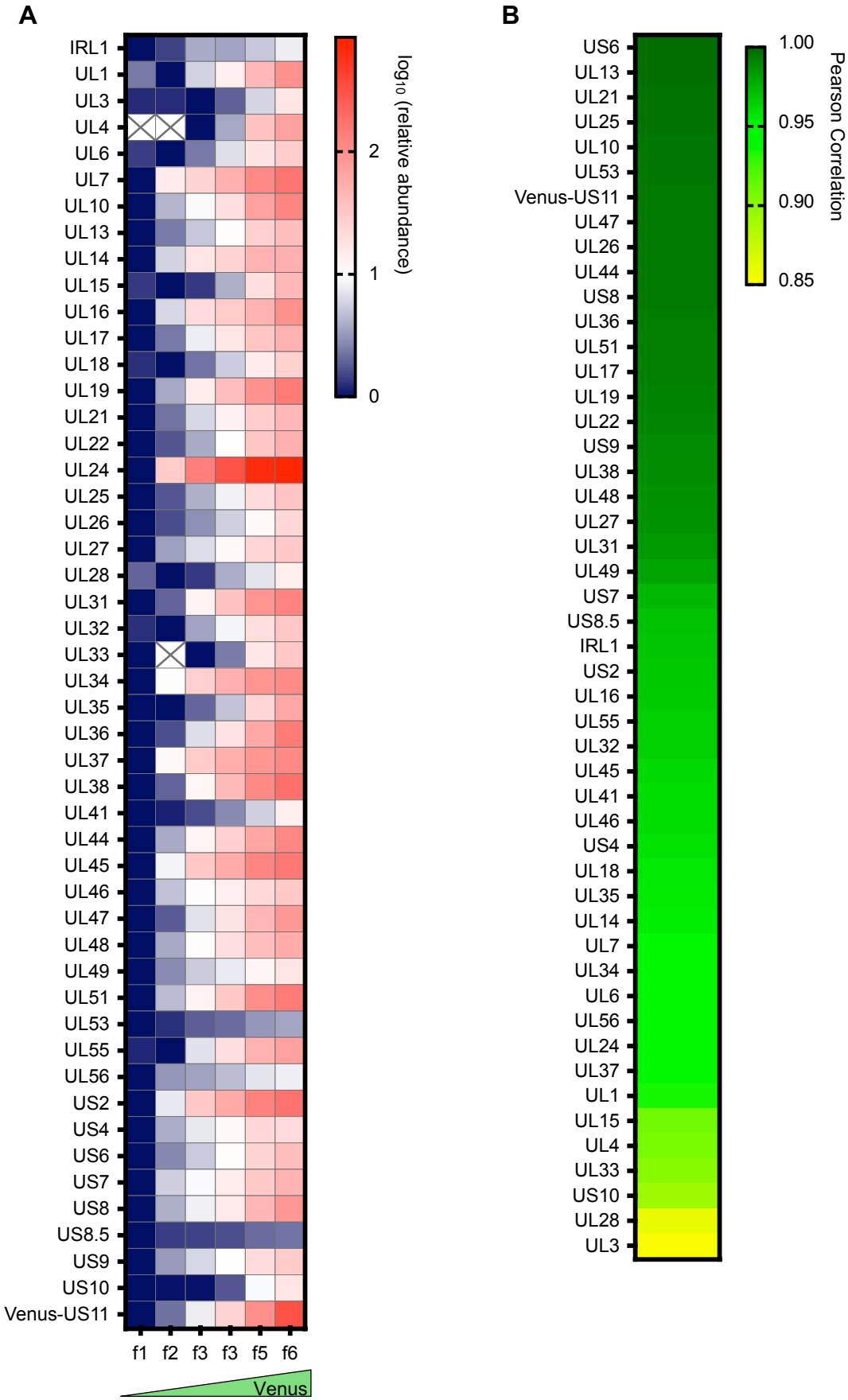

Fig. 2 M. Nobe and Y. Maruzuru et al.

Fig. 2. Abundance of HSV-1 L proteins in each subpopulation of rICP47/vUs11-infected cells. (A) HeLa cells were infected for 24 h with rICP47/vUs11 at an MOI of 5 and sorted into six subpopulations (f1 to f6) by cell sorting as shown in S. Fig. 1A and each subpopulation was analyzed by LC-MS/MS. The heatmap of log10 (relative abundance) of 49 HSV-1 L proteins in each subpopulation is shown. X: not detectable. Peptides of UL4 were not detectable in subpopulations f1 and f2 and those of UL33 were not detectable in subpopulation f2. (B) Heatmap of the Pearson correlation coefficient between $\log_{10}$ (MFI of Venus) of each subpopulation and $\log_{10}$ (relative abundance) of each HSV-1 L protein. For UL4 and UL33, when peptides were not detected in the subpopulations above, Pearson correlation coefficients were calculated by completing missing values with 0. P-values for the correlation coefficient of all HSV-1 L proteins shown in B were < 0.05.

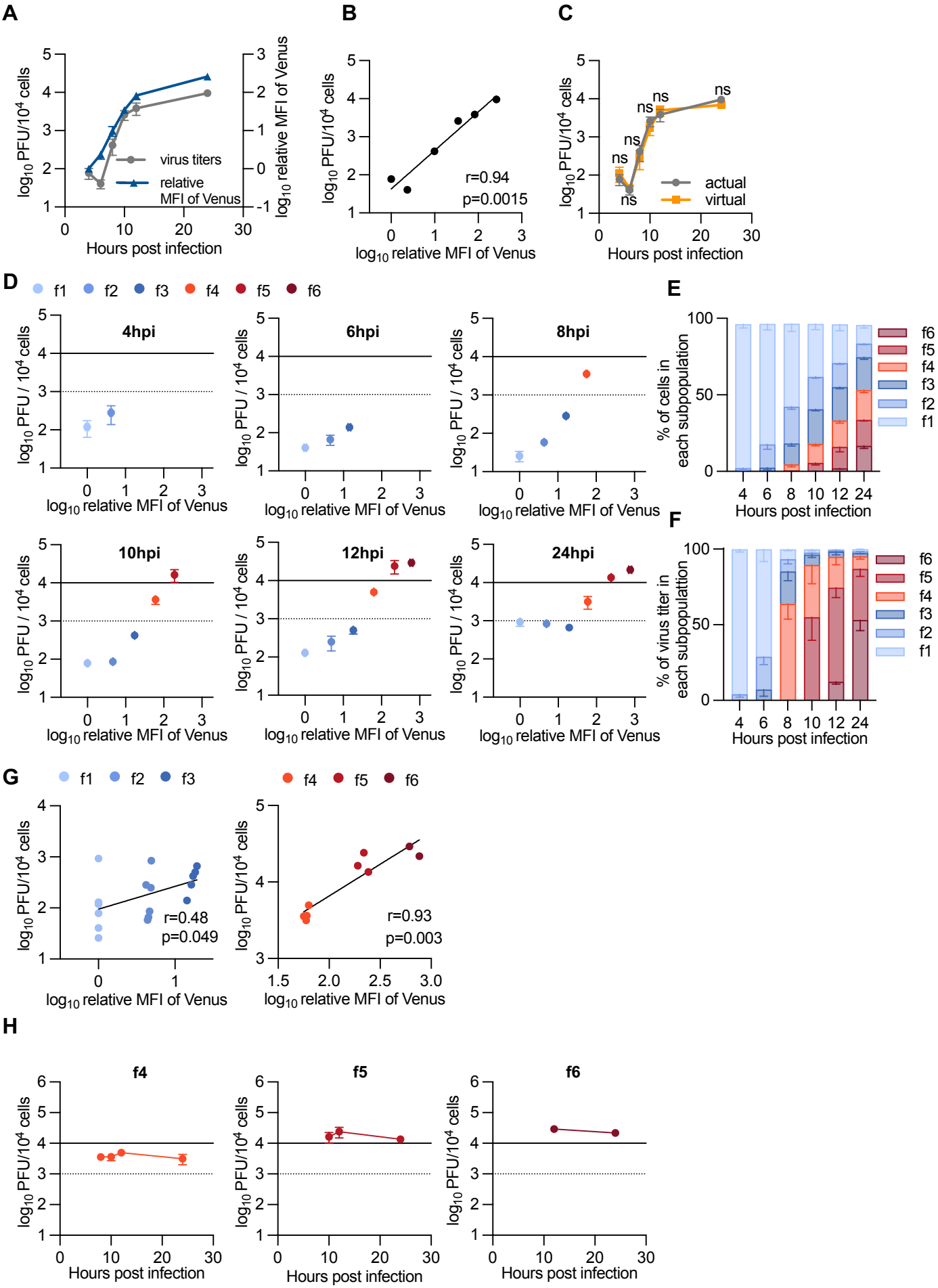

Fig. 3 M. Nobe and Y. Maruzuru et al.

Fig. 3. Quantitative analysis of a relationship between the expression levels of HSV-1 L proteins and progeny virus yields. (A to H) HeLa cells were infected with rICP47/vUs11 at an MOI of 5, analyzed by flow cytometry, and sorted into an entire cell population (FSC singlet) or f1 to f6 subpopulations by cell sorting at the indicated times after infection as shown in S. Fig.2. Sorted cells were sonicated and virus titers were determined by plaque assay using Vero cells. (A) Kinetics of mean fluorescent intensity (MFI) of Venus and progeny virus titers of the entire population. (B) Scatter plot of $\log_{10}$(relative MFI of Venus) vs $\log_{10}$(PFU/10^4 cells) from panel A. (C) Kinetics of progeny virus titers of the entire population from panel A (actual) and sum of the virus titers produced by each subpopulation (virtual). The calculation method for virtual titers is described in the Materials and methods. (D) Scatter plots of $\log_{10}$(relative MFI of Venus) vs $\log_{10}$(PFU/10^4 cells) of the indicated subpopulation separated by time after infection. (E) Proportion of cells in the indicated subpopulation account for the entire cell population at the indicated times after infection. (F) Proportion of virus titers produced by the f1 to f6 subpopulations account for virus titers produced by the entire population at the indicated times after infection. (G) Scatter plot of $\log_{10}$(relative MFI of Venus) vs $\log_{10}$(PFU/10^4 cells) of f1 to f3 (left), or f4 to f6 (right) subpopulations. The data are from panel D. (H) Progeny virus titers of the indicated subpopulations at the indicated times after infection. The data are from panel D. Each value is the mean ± standard error (A, C, D, E, F, and H) or mean (B and G) of the results of three independent experiments. Statistical analysis was performed by unpaired Student's *t*-test. ns, not significant (C). Solid and dashed lines indicate 1 PFU/cell and 0.1 PFU/cell, respectively (D and H).

A

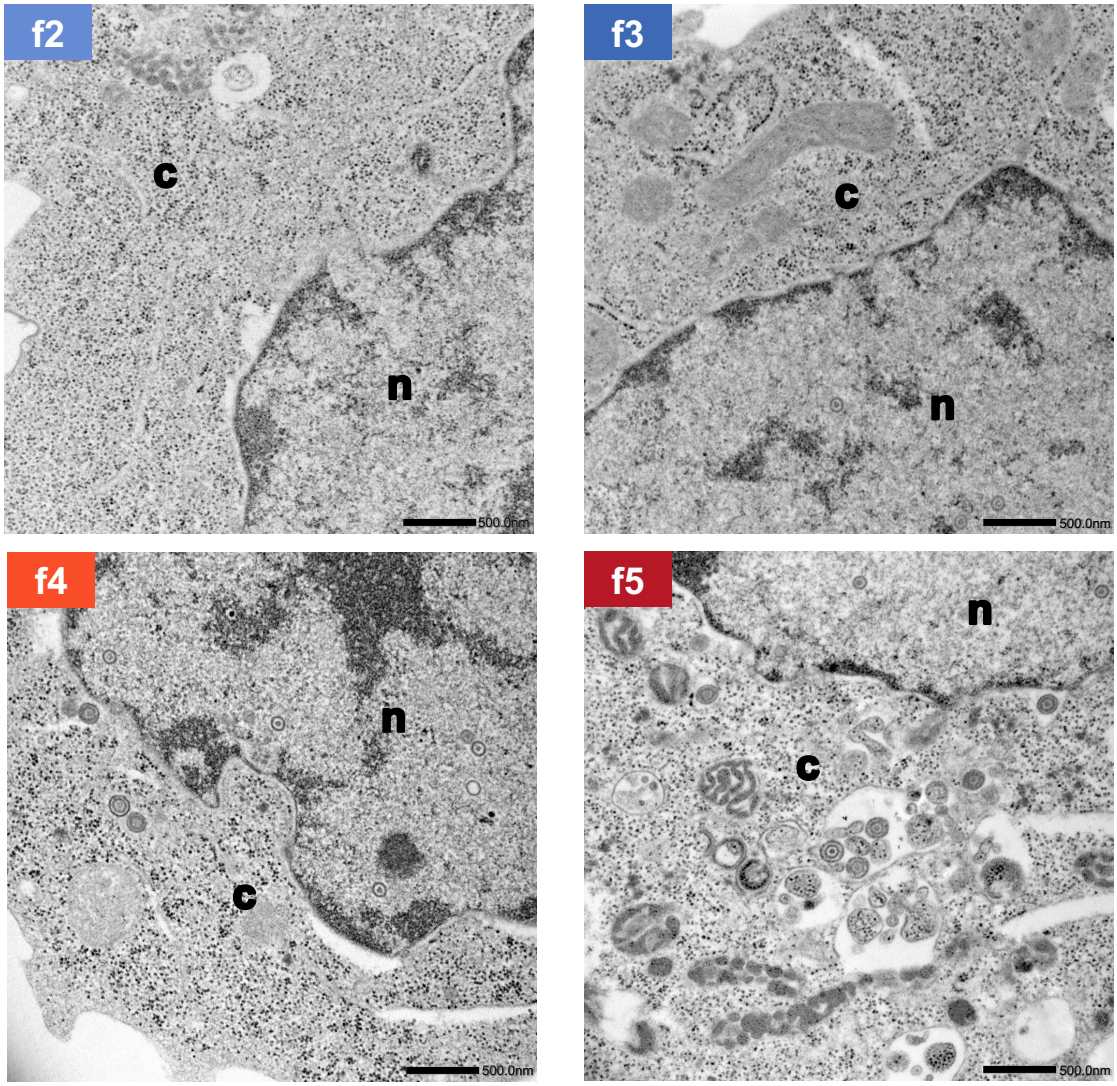

B

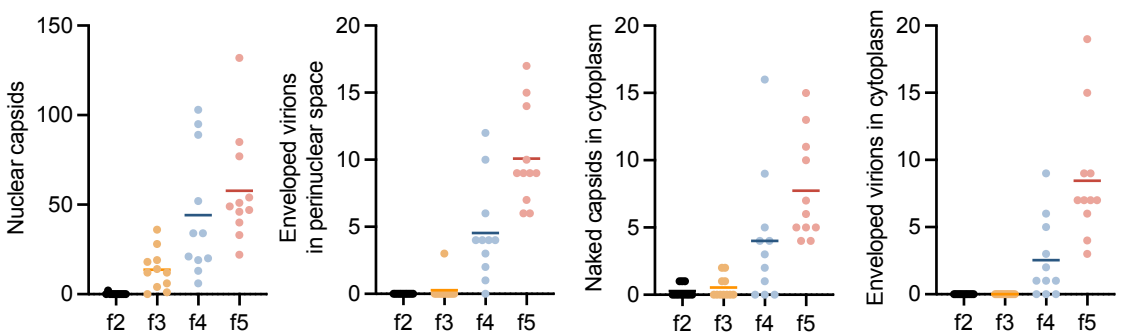

Fig. 4. Electron microscopic analysis of cells in the f2 to f5 subpopulations. (A and B) HeLa cells were infected with rICP47/vUs11 at an MOI of 5 and sorted into four subpopulations (f2 to f5) by cell sorting 24 h after infection. Sorted cells were fixed, embedded, sectioned, stained, and examined by electron microscopy. (A) A transmission electron microscopy image of cells in the f2 to f5 subpopulations. n, nucleus; c, cytoplasm. Scale bars = 500 nm. (B) The numbers of nuclear virions, enveloped virions in the perinuclear space, naked capsids in the cytoplasm, and enveloped virions in the cytoplasm of 10 cells in the f2 to f5 subpopulations were quantitated. The horizontal bars indicate the means.

Fig. 4 M. Nobe and Y. Maruzuru et al.

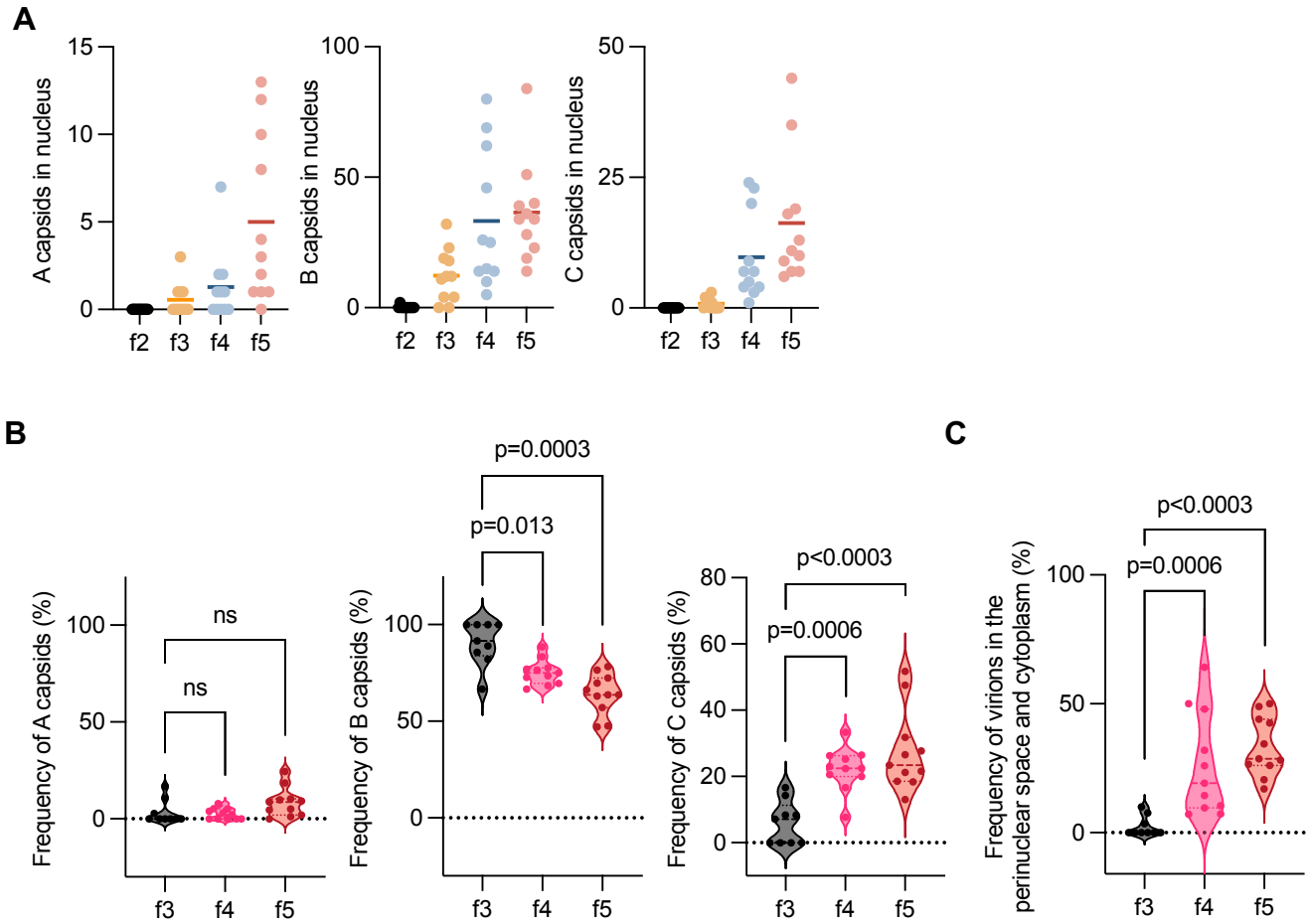

Fig. 5. Frequencies of A, B, and C capsids in the nucleus of cells in the f2 to f5 subpopulations. (A) The numbers of A, B, and C capsids in the nucleus of 11 cells analyzed in Fig. 4 in the f2 to f5 subpopulations were quantitated. The horizontal bars indicate the means ± standard errors. Proportions of A, B, and C capsids to nuclear capsids (B), or virions in the perinuclear space and cytoplasm (C) of cells with more than two nuclear capsids (f3, n = 9; f4, n = 11; f5, n = 11). Data are presented as the median ± interquartile range (IQR). Statistical analysis was performed by the Mann-Whitney *U*-test, and P-values were adjusted by Bonferroni correction. ns, not significant.

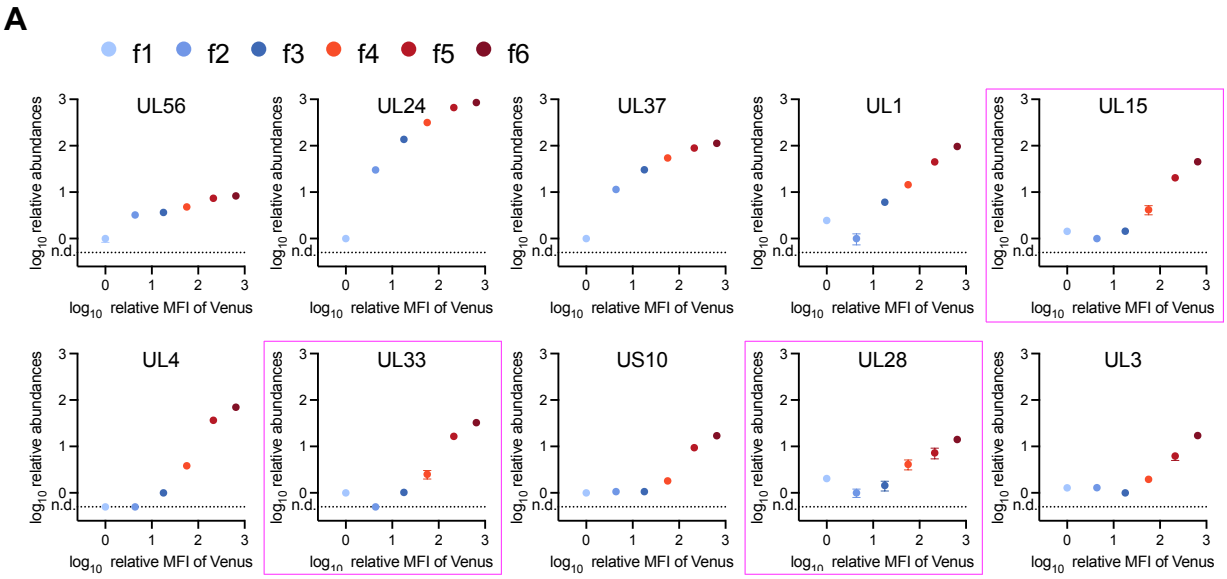

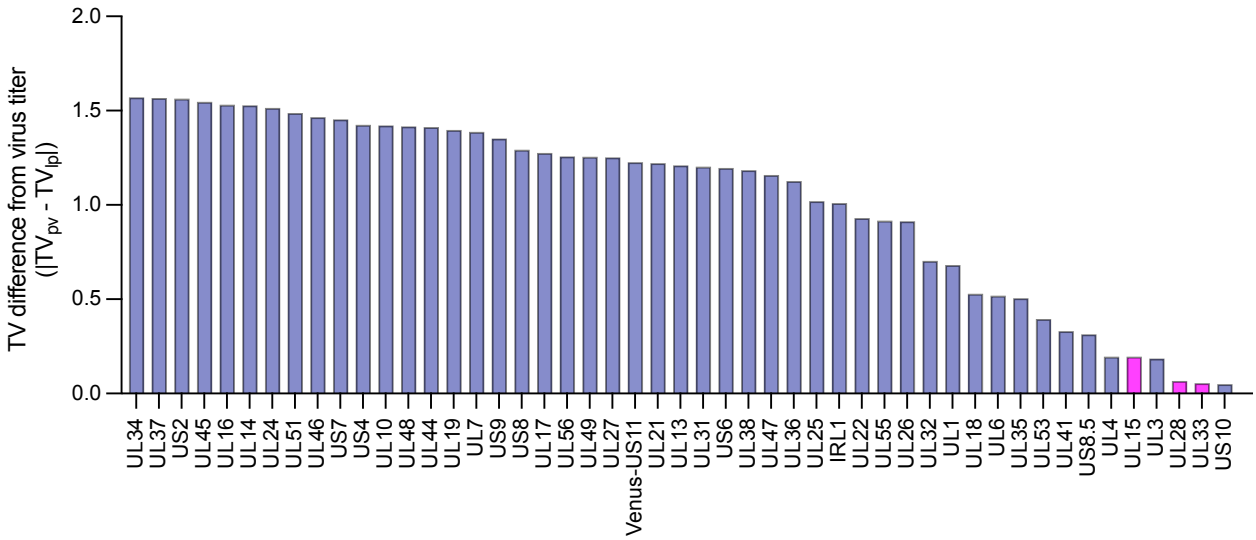

Fig. 6. Abundance of 10 HSV-1 L proteins in each subpopulation of rICP47/vUs11 infected cells. (A) Scatter plots of $\log_{10}$(relative MFI of Venus) vs $\log_{10}$(relative abundance) of L proteins (from S. Fig. 1B) of the bottom 10 HSV-1 L proteins with relatively low correlation coefficients between fluorescence intensity of Venus and their abundance (from Fig. 2B). Plots of terminase subunits are marked with magenta squares. (B) Difference between the TV of progeny virus production (TVpv) (from S. Fig 6A) and TV of 40 L proteins (TVlp) (from S. Fig. 6B). Data of terminase subunits are shown in magenta.